

A Luminescent Zirconium(IV) Complex as a Molecular Photosensitizer for Visible Light Photoredox Catalysis

Yu Zhang, Jeffrey L. Petersen, and Carsten Milsmann*

C. Eugene Bennett Department of Chemistry, West Virginia University, 100 Prospect Street, Morgantown, West Virginia 26506, United States

S Supporting Information

ABSTRACT: Titanium and zirconium complexes carrying two 2,6-bis(pyrrolyl)pyridine ligands have been synthesized and characterized. The neutral complexes $\text{Ti}(\text{MePDP})_2$ and $\text{Zr}(\text{MePDP})_2$ (MePDP = 2,6-bis(5-methyl-3-phenyl-1H-pyrrol-2-yl)pyridine) show intense ligand-to-metal charge-transfer bands in the visible region and undergo multiple reversible redox events under highly reducing conditions. $\text{Zr}(\text{MePDP})_2$ exhibits photoluminescent behavior and its excited state can be quenched by mild reductants to generate a powerful electron transfer reagent with a ground state potential of -2.16 V vs $\text{Fc}^{+/0}$. This reactivity was utilized to facilitate dehalogenation reactions, the reduction of electron-poor olefins, and the reductive coupling of benzyl bromide via photoredox catalysis. In these reactions, the earth-abundant metal complex $\text{Zr}(\text{MePDP})_2$ acts as a substitute for the precious metal photosensitizer $[\text{Ru}(\text{bpy})_3]^{2+}$.

Photoluminescent transition metal complexes have received considerable attention due to their importance in photovoltaic devices,¹ solar fuel production,² and photoredox catalysis.³ A common design element of many popular, metal-based molecular photosensitizers is the combination of an electron-rich metal center with strong π -acceptor ligands. In these complexes, initial charge separation occurs via metal-to-ligand charge-transfer (MLCT) transitions often followed by intersystem crossing (ISC) leading to long-lived excited states.⁴ The light energy stored in the luminescent excited state alters the redox-potentials of the photosensitizer and enables facile single-electron transfer (SET) reactions. Prominent examples for this type of photosensitizer are $[\text{Ru}^{\text{II}}(\text{bpy})_3]^{2+}$ (d^6 , bpy = 2,2'-bipyridine),⁵ $[\text{Ir}^{\text{III}}(\text{ppy})_3]$ (d^6 , ppy = 2,2'-phenylpyridine),⁶ and $[\text{Cu}^{\text{I}}(\text{dmp})_2]^{1+}$ (d^{10} , dmp = 2,9-dimethyl-1,10-phenanthroline)⁷ as well as the more recently reported complexes $\text{W}^0(\text{C}\equiv\text{NAr})_6$ (d^6 , Ar = 2,6-dimethylphenyl)⁸ and $[\text{Pt}^{\text{II}}(\text{terpy})(\text{C}\equiv\text{CR})]^{1+}$ (d^8 , terpy = 2,2';6',2''-terpyridine).⁹ A notable exception are cerium(III) amide and guanidinate complexes recently reported by Schelter et al., in which the strong luminescence originates from $5d \rightarrow 4f$ transitions.¹⁰

Ligand-to-metal charge transfer (LMCT) presents an alternative strategy for the design of photoactive transition metal compounds. Among the most well-studied examples are cyclopentadienyl complexes of d^0 metal ions.¹¹ However, most of these complexes require excitation with UV rather than visible light. Luminescent LMCT states from visible light excitation

have been observed in group 5 and 6 complexes carrying a single oxo or imido ligand.¹² Electron rich metal complexes with luminescent LMCT states have been reported for Re and Tc using bidentate phosphine ligands.¹³ Our interest in this type of mechanism was sparked by the potential to develop molecular photosensitizers based on group 4 transition metals. The high earth-abundance and the resulting low cost of titanium and zirconium as the second and fourth most-abundant transition metals in the earth's crust, respectively,¹⁴ makes these metals attractive candidates for large-scale solar energy applications.¹⁵ Herein, we present a new molecular photosensitizer based on the electron-deficient early transition metal Zr(IV) and a π -donating pyridine dipyrrolyde, PDP, ligand and demonstrate its utility in photoredox catalysis.

Transition metal complexes using a pincer-type 2,6-bis(pyrrolyl)pyridine ligand framework were only recently reported.¹⁶ This ligand architecture exhibits a number of attractive features for the design of LMCT photosensitizers: (a) Pyrrolyde ligands are π -donors due to the amide character of the nitrogen atom and the 2,2'-connectivity between the pyrrolyde and pyridine rings confers amide character to the pyridine nitrogen via conjugation; (b) the extended π -system allows for facile charge delocalization and the ligand was shown to be readily oxidized by up to two electrons;^{16b} (c) the pincer-type backbone provides a rigid framework for the synthesis of coordinatively saturated octahedral complexes and its modular synthesis allows for straightforward tuning of the steric and electronic properties of the ligand. For the purpose of this study, we focused on 2,6-bis(5-methyl-3-phenyl-1H-pyrrol-2-yl)pyridine, $\text{H}_2^{\text{MePDP}}$, which was synthesized from commercially available 2,6-pyridinedicarbaldehyde and benzylideneacetone via a straightforward two step/one pot protocol.¹⁷

Addition of two equivalents of $n\text{-BuLi}$ to $\text{H}_2^{\text{MePDP}}$ resulted in clean deprotonation yielding $\text{Li}_2^{\text{MePDP}}$. Treatment of ZrCl_4 with two equivalents of $\text{Li}_2^{\text{MePDP}}$ at room temperature provided $\text{Zr}(\text{MePDP})_2$ in 69% yield (Scheme 1). A similar protocol using $\text{TiCl}_4(\text{thf})_2$ as the metal precursor did not furnish the corresponding titanium complex, but led to the formation of unidentified paramagnetic products. This reactivity is probably due to facile reduction of Ti^{IV} by the lithium salt of the ligand. In contrast, reaction of $\text{TiCl}_3(\text{thf})_3$ with two equivalents of $\text{Li}_2^{\text{MePDP}}$ resulted in clean formation of paramagnetic $[\text{Li}(\text{thf})_4][\text{Ti}(\text{MePDP})_2]$ in 62% yield, which was converted to $\text{Ti}(\text{MePDP})_2$ by oxidation with half an equivalent of I_2 (92%

Received: June 9, 2016

Published: September 19, 2016

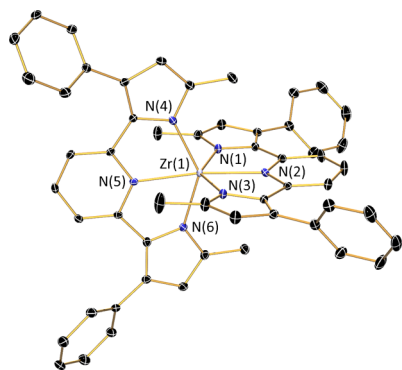
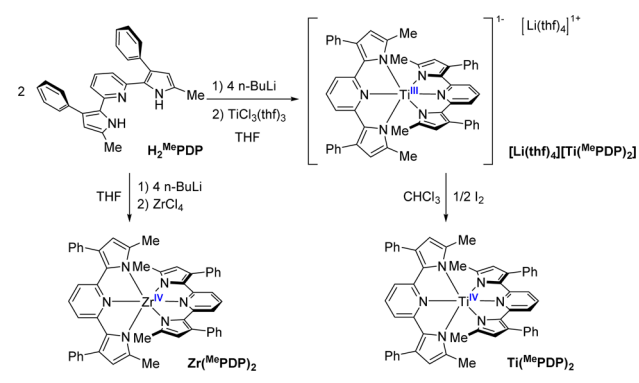
Scheme 1. Synthesis of $Zr^{(Me)PDP}_2$, $Ti^{(Me)PDP}_2$, and $[Li(thf)_4][Ti^{(Me)PDP}_2]$


Figure 1. Representation of the molecular structure of $Zr^{(Me)PDP}_2$ with 50% probability ellipsoids. Hydrogen atoms were omitted for clarity.

yield). The molecular structures of the three complexes were established by X-ray diffraction and the structure of $Zr^{(Me)PDP}_2$ is shown in Figure 1. In all complexes, the coordination environment around the central metal ion is best described as distorted octahedral with two meridionally coordinating tridentate $^{Me}PDP^{2-}$ ligands. The geometric constraints enforced by the ligand framework result in reduced average $N_{pyrrol}-M-N_{pyrrol}$ angles of $140.00(9)^\circ$, $147.57(11)^\circ$, and $149.40(9)^\circ$ for the pincer ligands in $Zr^{(Me)PDP}_2$, $Ti^{(Me)PDP}_2$, and $[Ti^{(Me)PDP}_2]^{1-}$, respectively. The two tridentate ligands exhibit nearly perfect perpendicular orientation in all complexes as indicated by the angle between the $N(1)-N(2)-N(3)$ and the $N(4)-N(5)-N(6)$ planes. The 1H NMR spectroscopy data for diamagnetic $Zr^{(Me)PDP}_2$ and $Ti^{(Me)PDP}_2$ as well as for paramagnetic $[Li(thf)_4][Ti^{(Me)PDP}_2]$ are in agreement with D_{2d} symmetric structures in solution. No significant changes in the intraligand bond distances are observed between $Ti^{(Me)PDP}_2$ and the one-electron reduced complex ion $[Ti^{(Me)PDP}_2]^{1-}$ (Table S1), indicating metal-centered reduction and a +III oxidation state for the titanium ion in $[Li(thf)_4][Ti^{(Me)PDP}_2]$. Consistent with this assignment, the average $Ti-N_{pyrrole}$ bond length increases from 2.039(3) Å in the neutral complex to 2.113(2) Å in the anionic compound. The average $Ti-N_{pyridine}$ distance remains constant with 2.122(3) Å and 2.129(2) Å in $Ti^{(Me)PDP}_2$ and $[Ti^{(Me)PDP}_2]^{1-}$, respectively.

Despite their structural similarities, the optical properties of the neutral complexes $Zr^{(Me)PDP}_2$ and $Ti^{(Me)PDP}_2$ are quite different. Solutions of $Ti^{(Me)PDP}_2$ in THF exhibit a dark brown color without any visible luminescence under ambient light or upon irradiation with UV light at 365 or 254 nm. In contrast, THF solutions of the zirconium analog show an intense pink

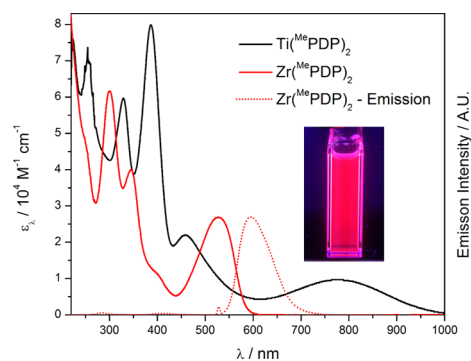


Figure 2. Absorption spectra of $Ti^{(Me)PDP}_2$ and $Zr^{(Me)PDP}_2$ and emission spectrum of $Zr^{(Me)PDP}_2$ recorded in THF solution at room temperature. Inset: THF solution of $Zr^{(Me)PDP}_2$ under UV irradiation (365 nm).

color and are photoluminescent. Electronic absorption spectra for both complexes as well as the emission spectrum of $Zr^{(Me)PDP}_2$ upon excitation at 528 nm are shown in Figure 2. The spectrum of $Ti^{(Me)PDP}_2$ exhibits two absorption bands above 400 nm with maxima at 777 nm ($\epsilon = 9\,669\,M^{-1}\,cm^{-1}$) and 459 nm ($\epsilon = 22\,012\,M^{-1}\,cm^{-1}$), which are tentatively assigned as charge transfer bands based on their intensities. Even stronger absorption bands were observed in the UV region at 386 nm ($\epsilon = 79\,819\,M^{-1}\,cm^{-1}$), 330 nm ($\epsilon = 59\,659\,M^{-1}\,cm^{-1}$), and 255 nm ($\epsilon = 69\,944\,M^{-1}\,cm^{-1}$). No emission bands were detected upon excitation at wavelengths corresponding to these absorption maxima. The spectrum obtained for $Zr^{(Me)PDP}_2$ shows similar features with blue-shifted absorption maxima. A single absorption band was observed in the visible region with a maximum at 528 nm ($\epsilon = 27\,001\,M^{-1}\,cm^{-1}$). Additional bands with maxima at 346 nm ($\epsilon = 40\,028\,M^{-1}\,cm^{-1}$) and 300 nm ($\epsilon = 61\,582\,M^{-1}\,cm^{-1}$) are located in the UV part of the spectrum. A weaker absorption band is visible as a shoulder around 395 nm. Excitation at any of these wavelengths resulted in the detection of an emission spectrum with a maximum at 594 nm. A luminescence quantum yield, Φ , of 0.08 was determined via a comparative method using Rhodamine 6G in ethanol as the reference.¹⁸ This value is similar to the one reported for $[Ru(bpy)_3]^{2+}$ in acetonitrile ($\Phi = 0.09$) or water ($\Phi = 0.06$) under oxygen-free conditions.¹⁹

To establish the nature of the electronic transitions, time-dependent density functional theory (TD-DFT) calculations were performed at the B3LYP level of theory. Solvent effects were included using the conductor-like screening model (COSMO). The calculated absorption spectra are in good agreement with the experimental data (Figure 3 and Figure S40). The lowest energy band in both neutral complexes corresponds to a transition from an exclusively ligand centered π orbital (b_2 in D_{2d} symmetry) to a degenerate set of orbitals (e) with significant contributions from the metal (d_{xz} , d_{yz}) and the pyridine rings of the ligands (Figure 3). The metal character of the acceptor orbitals was found to be 61% in the case of $Ti^{(Me)PDP}_2$ and 34% for $Zr^{(Me)PDP}_2$ in agreement with significant LMCT contributions.

To investigate the potential for outer sphere electron transfer, cyclic voltammetry (CV) experiments were performed for $Ti^{(Me)PDP}_2$ and $Zr^{(Me)PDP}_2$ in THF using ferrocene, $Fc^{+/0}$, as an internal standard. For both compounds an irreversible oxidation event with a peak potential around 0.9 V was observed. This feature is readily assigned as an oxidation of the ligand

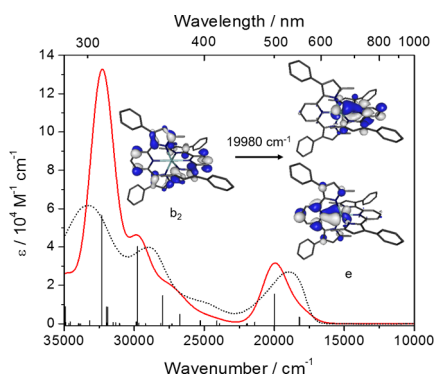
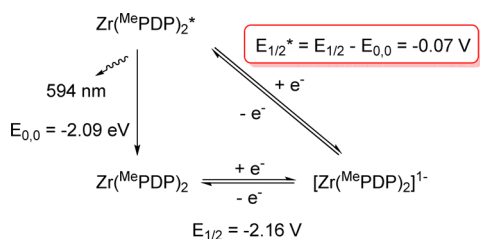


Figure 3. TD-DFT (COSMO) predicted electronic absorption spectrum of $\text{Zr}(\text{MePDP})_2$ (red line, fwhm of 2000 cm^{-1}). Vertical bars indicate the position of the predicted transitions. The experimental spectrum is shown as a dotted line for comparison. The orbital pictures represent the donor (b_2) and acceptor (e) orbitals for the calculated transitions in the visible region at $19\,980\text{ cm}^{-1}$ (500.5 nm).

framework followed by rapid decomposition of the oxidized product as metal centered oxidation reactions can be excluded for Ti^{IV} and Zr^{IV} complexes. More interestingly, both compounds undergo multiple reductions at negative potentials. The CV of $\text{Ti}(\text{MePDP})_2$ exhibits two fully reversible redox waves at -1.23 and -2.64 V followed by a quasi-reversible redox event at -3.16 V (Figure S20). For $\text{Zr}(\text{MePDP})_2$, reversible redox events were observed at -2.16 and -2.63 V with a quasi-reversible feature at -3.22 V (Figure S22). Based on the previously isolated complex $[\text{Ti}(\text{MePDP})_2]^{1-}$ and the strong dependence on the nature of the transition metal ion, the first reduction event can be tentatively assigned as a predominantly metal centered reduction. The more negative potential for Zr is in agreement with the generally more difficult reduction of second vs first row transition metals. The similar potentials for the second and third reduction events indicate primarily ligand centered reductions.

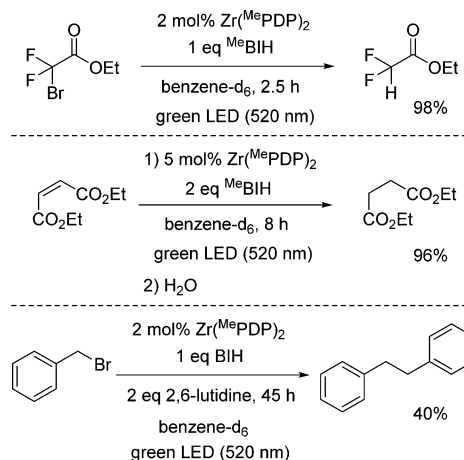
Having established the electrochemical properties of the ground state and the emission profile, the excited state potential for the redox-couple $\text{Zr}(\text{MePDP})_2^*/[\text{Zr}(\text{MePDP})_2]^{1-}$ was estimated as -0.07 V vs $\text{Fc}^{+/0}$ using the Rehm–Weller formalism (Scheme 2).²⁰ Based on this potential, 1,3-dimethyl-2-phenyl-

Scheme 2. Estimation of the Excited State Potential for $\text{Zr}(\text{MePDP})_2$



2,3-dihydro-1H-7-methylbenzo- $[d]$ imidazole, MeBIH , was identified as a potential reductant for $\text{Zr}(\text{MePDP})_2^*$. The redox potential for one-electron oxidation of MeBIH is slightly more negative (-0.16 V vs $\text{Fc}^{+/0}$ in MeCN) than the one reported for BIH (-0.10 V vs $\text{Fc}^{+/0}$ in MeCN),²¹ which is frequently used as a terminal reductant in photoredox reductions of organic substrates²² and CO_2 .²³ Addition of MeBIH to $\text{Zr}(\text{MePDP})_2$ in THF solution lead to a significant reduction of luminescence intensity indicating quenching of the excited state (Figure S13).

Scheme 3. Reaction Conditions for Photoredox Experiments



Encouraged by these results, the potential for photoredox catalysis using $\text{Zr}(\text{MePDP})_2$ as the photosensitizer was explored (Scheme 3). As a first proof of concept, the dehalogenation of ethyl bromodifluoroacetate was attempted. Photocatalytic dehalogenation reactions with organic hydride sources such as 1-benzyl-1,4-dihydronicotinamide (BNAH) or Hantzsch esters were among the earliest examples of photoredox reactions using the reductive quenching cycles of $[\text{Ru}(\text{bpy})_3]^{2+}$ or $\text{Ir}(\text{ppy})_3$.²⁴ Irradiation of an equimolar mixture of ethyl bromodifluoroacetate and MeBIH in benzene- d_6 in the presence of catalytic amounts of $\text{Zr}(\text{MePDP})_2$ with green LED light ($\lambda_{\text{max}} = 520\text{ nm}$) resulted in clean conversion to ethyl difluoroacetate and precipitation of MeBIHBr within 2.5 h. No reaction was observed in the absence of either light or $\text{Zr}(\text{MePDP})_2$. Additionally, no reaction was observed using $\text{Ti}(\text{MePDP})_2$ under irradiation with green or red LED light ($\lambda_{\text{max}} = 630\text{ nm}$). A second reductive transformation that has been well-established for precious metal photosensitizers in combination with BNAH is the reduction of electron-deficient olefins.²⁵ Employing the $\text{Zr}(\text{MePDP})_2/\text{MeBIH}$ system described herein, the reduction of diethyl maleate to diethyl succinate proceeded readily upon irradiation with green light for 8 h followed by aqueous work up. Again, no reduction was observed in the absence of zirconium catalyst or in the dark.

Although the two reactions described above clearly establish the photosensitizer properties of $\text{Zr}(\text{MePDP})_2$, excitation energy transfer to MeBIH followed by hydride transfer cannot be ruled out as a mechanistic alternative to the desired single-electron transfer pathway. Therefore, the reductive coupling of benzyl bromide to bibenzyl was investigated as an example for a reduction without net hydride transfer.^{7b,26} Initial experiments with $\text{Zr}(\text{MePDP})_2/\text{MeBIH}$ and benzyl bromide in benzene- d_6 resulted in poor conversion and decomposition of the zirconium catalyst. However, small amounts of bibenzyl were detected by ^1H NMR spectroscopy. The potential formation of HBr during turnover was identified as a likely reason for the observed catalyst decomposition via protonation of the pyrrolide arms of the ligand. In agreement with this hypothesis, addition of pyridine or 2,6-lutidine resulted in full conversion of benzyl bromide and an increased yield of the desired bibenzyl product (40%). The presence of benzylic C–H bonds in MeBIH could result in the formation of unintended byproducts. To examine this, we utilized alternative quenchers (BIH and ClBIH) that lack benzylic protons. Although the number of byproducts was decreased, slow conversion was observed. This can be attributed to the less

favorable potentials of BIH and ^{Cl}BIH for reduction of Zr(^{Me}PDP)₂*,²¹ which is supported by Stern–Volmer quenching experiments showing a clear correlation between quenching efficiency and redox potential (Table 1).

Table 1. Stern–Volmer Constants and Redox Potentials for ^RBIH Derivatives Used in Photoredox Reactions

	^{Me} BIH	BIH	^{Cl} BIH
E_{ox} (V vs Fc ^{+/0})	−0.16	−0.10	0.00
K_{SV} (L mol ^{−1})	47 900 ± 600	3500 ± 100	no quenching

In conclusion, we have developed a photoluminescent zirconium complex supported by 2,6-bis(pyrrolyl)pyridine ligands that acts as an earth-abundant metal substitute for precious metal photosensitizers in reductive photoredox catalysis using visible light. Experimental and computational studies of Zr(^{Me}PDP)₂ and its titanium analog suggest that the visible light absorption bands exhibit significant ligand-to-metal charge-transfer character.

■ ASSOCIATED CONTENT

Supporting Information

The Supporting Information is available free of charge on the ACS Publications website at DOI: 10.1021/jacs.6b05934.

Experimental and computational details, spectroscopic and electrochemical characterization (PDF)

Crystallographic data for C₂₈H₂₅Cl₂N₃ (CIF)

Crystallographic data for C₆₂H₅₈N₆O₂Ti (CIF)

Crystallographic data for C_{80.50}H₈₆LiN₆O₄Ti (CIF)

Crystallographic data for C_{58.50}H₅₂Cl₄N₆Zr (CIF)

■ AUTHOR INFORMATION

Corresponding Author

*camilsmann@mail.wvu.edu

Notes

The authors declare no competing financial interest.

■ ACKNOWLEDGMENTS

West Virginia University and the Don and Linda Brodie Resource Fund for Innovation are acknowledged for financial support. This work used X-ray crystallography (CHE-1336071) and NMR (CHE-1228336) equipment funded by the National Science Foundation.

■ REFERENCES

- (1) (a) Nazeeruddin, M. K.; Baranoff, E.; Grätzel, M. *Sol. Energy* **2011**, *85*, 1172. (b) Grätzel, M. *J. Photochem. Photobiol., C* **2003**, *4*, 145. (c) Hagfeldt, A.; Boschloo, G.; Sun, L.; Kloo, L.; Pettersson, H. *Chem. Rev.* **2010**, *110*, 6595.
- (2) For recent reviews, see the *Special Issue: Solar Fuels in: Chem. Soc. Rev.* **2013**, *42*, 2205.
- (3) (a) Xuan, J.; Xiao, W.-J. *Angew. Chem., Int. Ed.* **2012**, *51*, 6828. (b) Prier, C. K.; Rankic, D. A.; MacMillan, D. W. C. *Chem. Rev.* **2013**, *113*, 5322. (c) Yoon, T. P.; Ischay, M. A.; Du, J. *Nat. Chem.* **2010**, *2*, 527. (d) Zeitler, K. *Angew. Chem., Int. Ed.* **2009**, *48*, 9785. (e) Tucker, J. W.; Stephenson, C. R. J. *J. Org. Chem.* **2012**, *77*, 1617.
- (4) (a) McCusker, J. K. *Acc. Chem. Res.* **2003**, *36*, 876. (b) Yeh, A. T.; Shank, C. V.; McCusker, J. K. *Science* **2000**, *289*, 935.
- (5) Kalyanasundaram, K. *Coord. Chem. Rev.* **1982**, *46*, 159.
- (6) (a) King, K. A.; Spellane, P. J.; Watts, R. J. *J. Am. Chem. Soc.* **1985**, *107*, 1431. (b) Dixon, I. M.; Collin, J.-P.; Sauvage, J.-P.; Flamigni, L.; Encinas, S.; Barigelletti, F. *Chem. Soc. Rev.* **2000**, *29*, 385.

(7) (a) McMillin, D. R.; Buckner, M. T.; Ahn, B. T. *Inorg. Chem.* **1977**, *16*, 943. (b) Kern, J. M.; Sauvage, J. P. *J. Chem. Soc., Chem. Commun.* **1987**, 287, 546.

(8) Sattler, W.; Ener, M. E.; Blakemore, J. D.; Rachford, A. A.; Labeaume, P. J.; Thackeray, J. W.; Cameron, J. F.; Winkler, J. R.; Gray, H. B. *J. Am. Chem. Soc.* **2013**, *135*, 10614.

(9) Yang, Q.-Z.; Wu, L.-Z.; Wu, Z.-X.; Zhang, L.-P.; Tung, C.-H. *Inorg. Chem.* **2002**, *41*, 5653.

(10) (a) Yin, H.; Carroll, P. J.; Manor, B. C.; Anna, J. M.; Schelter, E. J. *J. Am. Chem. Soc.* **2016**, *138*, 5984. (b) Yin, H.; Carroll, P. J.; Anna, J. M.; Schelter, E. J. *J. Am. Chem. Soc.* **2015**, *137*, 9234.

(11) (a) Kenney, J. W.; Boone, D. R.; Striplin, D. R.; Chen, Y.; Hamar, K. B. *Organometallics* **1993**, *12*, 3671. (b) Loukova, G. V.; Huhn, W.; Vasiliev, V. P.; Smirnov, V. A. *J. Phys. Chem. A* **2007**, *111*, 4117. (c) Loukova, G. V.; Smirnov, V. A. *Chem. Phys. Lett.* **2000**, *329*, 437. (d) Loukova, G. V.; Starodubova, S. E.; Smirnov, V. A. *J. Phys. Chem. A* **2007**, *111*, 10928. (e) Loukova, G. V. *Chem. Phys. Lett.* **2002**, *353*, 244. (f) Yam, V. W.-W.; Qi, G.-Z.; Cheung, K.-K. *Organometallics* **1998**, *17*, 5448. (g) Patrick, E. L.; Ray, C. J.; Meyer, G. D.; Ortiz, T. P.; Marshall, J. A.; Brozik, J. A.; Summers, M. A.; Kenney, J. W. *J. Am. Chem. Soc.* **2003**, *125*, 5461. (h) Bruce, M. R. M.; Kenter, A.; Tyler, D. R. *J. Am. Chem. Soc.* **1984**, *106*, 639. (i) Loukova, G. V.; Vasiliev, V. P.; Milov, A. A.; Smirnov, V. A.; Minkin, V. I. *J. Photochem. Photobiol., A* **2016**, *327*, 6. (j) Pfennig, B. W.; Thompson, M. E.; Bocarsly, A. B. *Organometallics* **1993**, *12*, 649.

(12) (a) Heinselman, K. S.; Hopkins, M. D. *J. Am. Chem. Soc.* **1995**, *117*, 12340. (b) Choing, S. N.; Francis, A. J.; Clendenning, G.; Schuurman, M. S.; Sommer, R. D.; Tamblyn, I.; Weare, W. W.; Cuk, T. J. *Phys. Chem. C* **2015**, *119*, 17029. (c) Tonks, I. A.; Durrell, A. C.; Gray, H. B.; Bercaw, J. E. *J. Am. Chem. Soc.* **2012**, *134*, 7301.

(13) (a) Chatterjee, S.; Del Negro, A. S.; Smith, F. N.; Wang, Z.; Hightower, S. E.; Sullivan, B. P.; Heineman, W. R.; Seliskar, C. J.; Bryan, S. A. *J. Phys. Chem. A* **2013**, *117*, 12749. (b) Adams, J. J.; Arulsamy, N.; Sullivan, B. P.; Roddick, D. M.; Neuberger, A.; Schmehl, R. H. *Inorg. Chem.* **2015**, *54*, 11136.

(14) Yaroshevsky, A. A. *Geochem. Int.* **2006**, *44*, 48.

(15) Radivojevic, I.; Bazzan, G.; et al. *J. Phys. Chem. C* **2012**, *116*, 15867.

(16) (a) Searles, K.; Fortier, S.; Khusniyarov, M. M.; Carroll, P. J.; Sutter, J.; Meyer, K.; Mendiola, D. J.; Caulton, K. G. *Angew. Chem., Int. Ed.* **2014**, *53*, 14139. (b) Komine, N.; Buell, R. W.; Chen, C.-H.; Hui, A. K.; Pink, M.; Caulton, K. G. *Inorg. Chem.* **2014**, *53*, 1361.

(17) (a) Nagata, T.; Tanaka, K. *Bull. Chem. Soc. Jpn.* **2002**, *75*, 2469. (b) Jones, R. A.; Karatza, M.; Voro, T. N.; Civeir, P. U.; Franck, A.; Ozturk, O.; Seaman, J. P.; Whitmore, A. P.; Williamson, D. J. *Tetrahedron* **1996**, *52*, 8707.

(18) (a) Brouwer, A. M. *Pure Appl. Chem.* **2011**, *83*, 2213. (b) Würth, C.; Grabolle, M.; Pauli, J.; Spieles, M.; Resch-Genger, U. *Nat. Protoc.* **2013**, *8*, 1535.

(19) Suzuki, K.; Kobayashi, A.; Kaneko, S.; Takehira, K.; Yoshihara, T.; Ishida, H.; Shiina, Y.; Oishi, S.; Tobita, S. *Phys. Chem. Chem. Phys.* **2009**, *11*, 9850.

(20) Rehm, D.; Weller, A. *Isr. J. Chem.* **1970**, *8*, 259.

(21) Zhu, X.-Q.; Zhang, M.-T.; Yu, A.; Wang, C.-H.; Cheng, J.-P. *J. Am. Chem. Soc.* **2008**, *130*, 2501.

(22) Hasegawa, E.; Tateyama, M.; Hoshi, T.; Ohta, T.; Tayama, E.; Iwamoto, H.; Takizawa, S. Y.; Murata, S. *Tetrahedron* **2014**, *70*, 2776.

(23) Yamazaki, Y.; Takeda, H.; Ishitani, O. *J. Photochem. Photobiol., C* **2015**, *25*, 106.

(24) (a) Fukuzumi, S.; Mochizuki, S.; Tanaka, T. *J. Phys. Chem.* **1990**, *94*, 722. (b) Nguyen, J. D.; D'Amato, E. M.; Narayanan, J. M. R.; Stephenson, C. R. J. *Nat. Chem.* **2012**, *4*, 854.

(25) Pac, C.; Ihama, M.; Yasuda, M.; Miyachi, Y.; Sakurai, H. *J. Am. Chem. Soc.* **1981**, *103*, 6495.

(26) Hironaka, K.; Fukuzumi, S.; Tanaka, T. *J. Chem. Soc., Perkin Trans. 2* **1984**, 1705.